Advanced Robotics, Vol. 20, No. 1, pp. 93–113 (2006)

Also available online - www.vsppub.com

Full paper

Back handspring of a multi-link gymnastic robot — reference model approach

SANG-HO HYON [1,*], NAOTO YOKOYAMA [2] and TAKASHI EMURA [1]

[1] *Department of Bioengineering and Robotics, Graduate School of Engineering, Tohoku University, Aramaki-Aza-Aoba 01, Aoba-ku, Sendai 980-8579, Japan*
[2] *Makino Corp., Nakane 2-3-19, Meguro-ku, Tokyo 152-8578, Japan*

Received 5 November 2004; accepted 14 February 2005

Abstract—This paper reports on the first gymnastic robot that can perform back handspring. The robot is a planar and serially connected four-link robot, with its joints actuated by electric servomotors. The paper describes the modeling of the robot and the control framework for a back handspring. The controller is derived from a task-specific reference model and its model matching. The use of a reference model described by global physical quantities such as center of mass or angular momentum allows the gymnastic motion planning of a multi-body system to be intuitive and the model matching controller can be applied directly to the experimental model without obtaining each joint trajectory. The controller effectiveness is confirmed *via* simulations and experiments of the back handspring. Although there remains the problem of how to systematically design the control parameters, the paper shows the strength of the model-based controller for fast gymnastic motions.

Keywords: Gymnastic robot; back handspring; jumping; non-linear control; reference model.

1. INTRODUCTION

Realization of complex and fast motion tasks is an important and attractive area of research. Such motion tasks enhance the mobility of humanoid robots and also contribute to the better understanding of human motor control. Gymnastic motion is included in such interesting motion tasks. This paper describes a gymnastic robot that can perform jumps, somersaults and back handsprings (Fig. 1).

Some studies have addressed gymnastic robots. Raibert *et al*. succeeded in jumping and somersault control of a three-dimensional bipedal robot [1, 2]. In the somersault, the robot undertakes rotational motion in flight, as well as translational motion (jumping). How much the robot rotates in the air depends on the angular momentum around the center of mass (CM) at lift-off and the inertia around the

*To whom correspondence should be addressed. E-mail: sangho@ieee.org

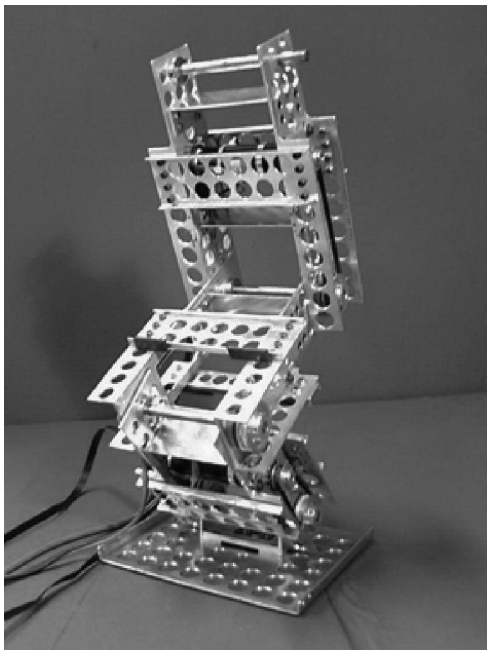

Figure 1. Four-link planar gymnastic robot.

CM during the flight. Analysis of the dynamics shows that we can control the initial angular momentum by the extension force of the leg for a given distance between the hip joint and the CM of the body. Furthermore, we can control the rotation speed by extending or retracting the legs in mid-flight. We depend greatly on model dynamics to obtain complex gymnastic performances for an articulated and multi-link structured model.

However, there is also an example in which jumping of the five-link robot was performed by numerically solving a two-point boundary problem to obtain joint trajectories and then applying high-gain local feedback control to each joint [3].

When humans perform gymnastic motions, feed-forward control with learning may play a dominant role. However, as long as that learning is based on sensory information, feedback controllers can give important insights into the learning mechanism, especially when the motion is generated only by a feedback controller. Moreover, feedback controllers have their own advantages over feed-forward ones — one of them being robustness against sudden environmental change.

In this context, there are some successful examples of a high bar robot using real-time feedback controllers. Spong and Yamakita *et al*. realized swing-up and balancing control [4, 5]. Nakanishi *et al*. succeeded in brachiating control of a two-link robot [6]. Recently, Yamakita *et al*. demonstrated a continuous motion of swing up → giant → somersault → landing → balancing using a multi-link robot [7]. Non-linear feedback control is also effective for jumping and flipping motions.

For example, Berkemeier and Fearing applied the feedback linearization technique to an underactuated robot (whose foot can freely rotate as a pivot joint) [8]. They found zero dynamics, which result from partial feedback linearization, to produce a periodic hopping or flipping motion. The same approach was found in [9].

This paper is intended to propose a control framework and a robotic test bed to study skill control in gymnastic motions [10]. For that purpose, a planar robot model is considered. The robot has 3 d.o.f., which can describe the 'global dynamics' of planar gymnastic motions, as described later.

The control strategy in this paper is to impose some reference model that describes gymnastic motions, especially for floor exercises, and realize them by a model matching controller. We expect the use of global physical quantities such as the CM or angular momentum to allow even a simple reference model to generate complex gymnastic motions of a multi-body system.

2. ROBOT MODEL

2.1. Mechanical model development

Figure 1 shows the newly developed planar gymnastic robot. The robot has four links that are connected serially by three joints. Each joint is actuated by a geared servomotor (20 W; Maxon Precision Motors) through a timing belt. The total reduction ratio for each joint is 10.8. Most of the mechanical parts are machined out of an aluminum frame. The overall height of the robot is 0.46 m; its total weight is 1.74 kg. Table 1 summarizes the physical parameters. Note that there is no 'boom' to constrain the robot to the sagittal plane.

Figure 2 shows the computer and electric system. The controller can run in real-time on a Linux PC (Pentium III 500 MHz) with a 1.3-ms control period. Servomotors are driven by DC servo-drivers with the torque control mode. The command signal to the servo-driver is sent by the DA converter. Joint angles are obtained by encoders mounted to the servomotors *via* a digital I/O. The interface is provided by an ISA-bus interface board (RIF-01). The robot is connected to the

Table 1.
Link parameters

	No. (i)	1	2	3	4
Mass (kg)	m_i	0.135	0.626	0.533	0.579
Link length (m)	l_i	0.09	0.13	0.15	0.19
CM position (m)[a]	l_{ci}	0.074	0.031	0.55	0.086
Inertia (kg mm^2)	J_i	260	1200	880	1600

[a] The CM position is the distance between the CM of each link and their proximal joint. All principal axes of each link are nearly coincident with their center axes. The ankle height h is 0.03 m.

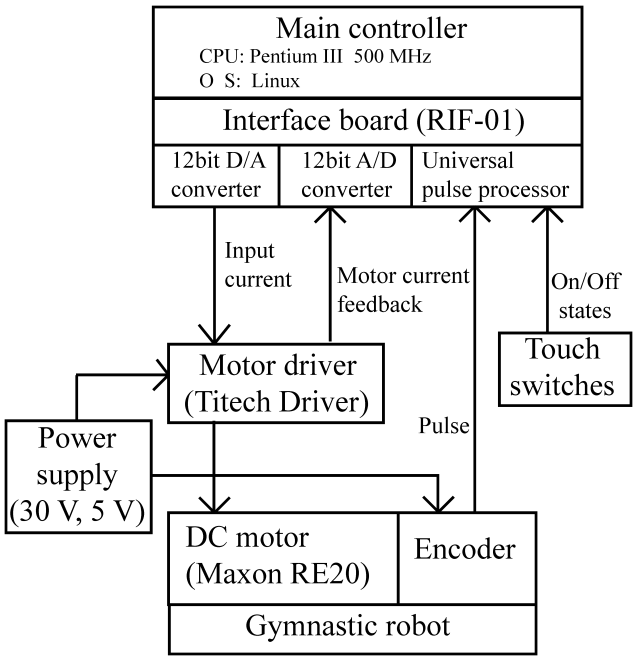

Figure 2. Computer and electric system.

computer and servo-drivers with cables. We use very light cables so that they do not disturb the robot's motion. Moreover, a gyro is not installed because the bandwith is not satisfactory for our purpose. Touch switches are attached to the floor to detect the ground contact of the robot.

2.2. Mathematical model representation

Figure 3 shows the definition of the mathematical model. Generalized coordinates include the absolute position to derive equations of motion for the stance phase and flight phase at once. That is, the generalized coordinates comprise (x_0, z_0), the toe position (x_g, z_g), the position of CM, as well as the joint angles ψ_i $(i = 1, 2, 3, 4)$, where ψ_1 is the attitude of the link 1 (foot), and ψ_2, ψ_3 and ψ_4 are the angles of the ankle, knee and hip, respectively. Control inputs are the joint torques, τ_2, τ_3 and τ_4. There is no torque applied around the toe $(\tau_1 = 0)$.

We assume that the foot neither bounces back nor slips on the ground (inelastic impulsive impact). This assumption is required to introduce an impulse equation. As shown in Fig. 4, a back handspring motion comprises successive phase transitions: Stance I (standing on the feet) $\rightarrow$ Flight II $\rightarrow$ Touchdown II $\rightarrow$ Stance II (standing on the head) $\rightarrow$ Touchdown I $\rightarrow \cdots$. It is similar to the phase transition of a running motion. Impulse equations describe the motions of the touchdown phases. When a human performs a back handspring, thanks to their hyper-multi-link struc-

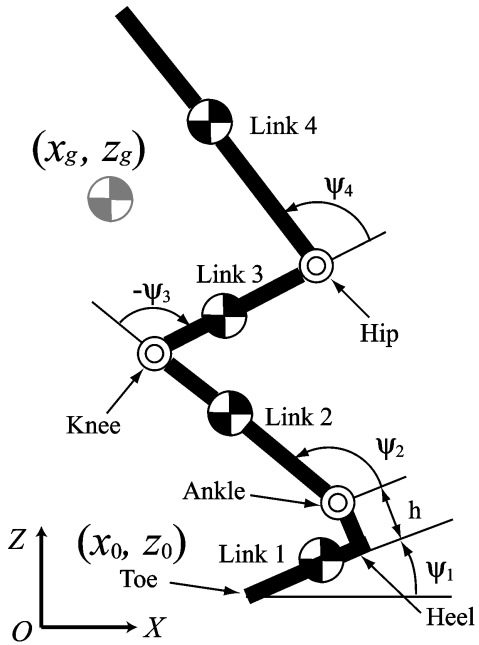

Figure 3. Definition of the mathematical model.

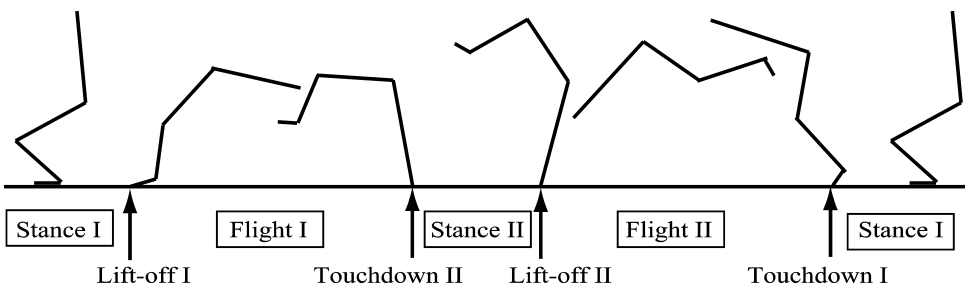

Figure 4. Phase transition of the back handspring.

ture, the touchdown is very smooth and no 'chattering' occurs between the feet (or hands) and the floor.

We aim to achieve such a smooth touchdown, but do not want to make it unnecessarily complicated. Therefore, we introduce an inelastic impulse assumption. A soft mat covers the floor to provide for that assumption.

2.3. Equations of motion at Stance I

The equations of motion can be expressed by Lagrange's equation of motion with constraints. A CM-coordinate system is used so that the CM position appears explicitly in the mathematical representation. Using the generalized coordinates

$q_g = [x_g, z_g, \psi]^T \in R^6$, where $\psi := [\psi_1, \psi_2, \psi_3, \psi_4]^T \in R^4$, the equation of motion can be expressed as:

$$J_g(q_g)\ddot{q}_g + H_g(q_g, \dot{q}_g) + G_g(q_g) = u + E_g(q_g)^T\lambda_g, \tag{1}$$

$$E_g(q_g)\dot{q}_g = 0. \tag{2}$$

Details of the inertial matrix $J_g(q_g) \in R^{6\times6}$, non-linear term $H_g(q_g, \dot{q}_g) \in R^6$ and gravity term $G_g(q_g) \in R^6$ are provided in the Appendix. The generalized force $u \in R^6$ is represented as:

$$u = \begin{bmatrix} 0_{3\times1} \\ \tau \end{bmatrix}, \tag{3}$$

which includes $\tau = [\tau_2, \tau_3, \tau_4]^T \in R^3$. The matrix $E_g(q_g)$ represents the derivative of the constraints as shown below.

As the constraint of the heel contact is defined as:

$$\Phi_0(q) = \begin{bmatrix} x_0 \\ z_0 \\ \psi_1 \end{bmatrix} = 0, \tag{4}$$

the time differentiation of the equation:

$$\frac{d}{dt}\Phi_0(q) = \left[\begin{array}{c|c} I_{2\times2} & -\frac{1}{M}J_{12} \\ \hline 0_{1\times2} & 1\ 0\ 0\ 0 \end{array}\right]\dot{q}_g = E_g(q_g)\dot{q}_g = 0, \tag{5}$$

yields (2), where $M = m_1 + m_2 + m_3 + m_4$ is the total mass and the matrix $J_{12} \in R^{2\times4}$ is defined in the Appendix. In this case, $E_g(q_g) \in R^{3\times6}$.

However, for toe contact, the constraint becomes:

$$\Phi_1(q) = \begin{bmatrix} x_0 \\ z_0 \end{bmatrix} = 0. \tag{6}$$

Its time differentiation becomes:

$$\frac{d}{dt}\Phi_1(q) = \left[\begin{array}{c|c} I_{2\times2} & -\frac{1}{M}J_{12} \end{array}\right]\dot{q}_g = E_g(q_g)\dot{q}_g = 0. \tag{7}$$

In this case, $E_g(q_g) \in R^{2\times6}$.

The associated constraint forces (the ground reaction forces) are represented by $\lambda_g := (\lambda_x, \lambda_z, \lambda_\psi)^T \in R^3$ for heel contact or $\lambda_g := (\lambda_x, \lambda_z)^T \in R^2$ for toe contact. They can be calculated by combining (1) and (2), which yields:

$$\lambda_g = -(E_g J_g^{-1} E_g^T)^{-1}\big(\gamma + E_g J_g^{-1}(u - H_g - G_g)\big), \tag{8}$$

where $\gamma = \dfrac{\partial}{\partial q_g}(E_g(q_g)\dot{q}_g)\dot{q}_g$.

At the beginning of the motion the robot stands still and maintains the constraint condition (4). Then, if the zero crossing of λ_ψ is detected, the heel takes off the ground and the constraint switches to (6).

From (A.9) and (A.10) in the Appendix, (1) is shown to have a decomposed structure of translational motion and rotary motion, as shown below:

$$\left[\begin{array}{cc|c} M & 0 & \\ 0 & M & 0_{(2\times 4)} \\ \hline \multicolumn{2}{c|}{0_{(4\times 2)}} & J_\psi(\psi) \end{array}\right] \left[\begin{array}{c} \ddot{x}_g \\ \ddot{z}_g \\ \hline \ddot{\psi} \end{array}\right] = \left[\begin{array}{c} 0 \\ -Mg \\ \hline H_\psi(\psi, \dot{\psi}) \end{array}\right]$$

$$+ \left[\begin{array}{cc|c} \multicolumn{2}{c|}{I_{2\times 2}} & 0_{2\times 1} \\ \hline & & 1 \\ -\frac{1}{M} J_{12} & & 0 \\ & & 0 \\ & & 0 \end{array}\right] \left[\begin{array}{c} \lambda_x \\ \lambda_z \\ \hline \lambda_\psi \end{array}\right] + \left[\begin{array}{c} 0 \\ 0 \\ \hline 0 \\ \tau \end{array}\right], \tag{9}$$

where g is the acceleration due to gravity. The matrix $J_\psi \in R^{4\times 4}$ and the vector $H_\psi \in R^4$ are shown in the Appendix. Note that λ_ψ in the second term in the right-hand side of (9) becomes zero in the case of toe contact.

2.4. Equations of motion at Flight I

The dynamics of the flight phase can be obtained easily by removing λ_g from (1), which yields:

$$J_g(q_g)\ddot{q}_g + H_g(q_g, \dot{q}_g) + G_g(q_g) = u. \tag{10}$$

2.5. Equations of motion at Touchdown I

The touchdown equation can be expressed as Lagrange's impulsive equation, which can be found in some classical dynamics textbooks [11]. The change of the generalized velocity just before and after touchdown $\Delta\dot{q} := \dot{q}_+ - \dot{q}_-$ can be calculated by the impulse equation with the constraint as

$$J_g(q_g)\Delta\dot{q}_g = E_g^T\hat{\lambda}_g, \tag{11}$$

$$E_g\dot{q}_{g+} = 0, \tag{12}$$

where E_g is the same matrix in (7) and $\hat{\lambda}_g \in R^2$ is the associated impulsive force, which can be calculated as:

$$\hat{\lambda}_g = -(E_g J_g^{-1} E_g^T)^{-1} E_g \dot{q}_{g-}. \tag{13}$$

Note that the touchdown contact occurs almost always at the toe or the head; hence, only $\Phi_1(q)$ is considered.

As in the case of Stance I, the impulse equation has a decomposed structure:

$$\left[\begin{array}{cc|c} M & 0 & \\ 0 & M & 0_{2\times 4} \\ \hline 0_{4\times 2} & & J_\psi \end{array}\right] \left[\begin{array}{c} \Delta\dot{x}_{\mathrm{g}} \\ \Delta\dot{z}_{\mathrm{g}} \\ \hline \Delta\dot{\psi} \end{array}\right] = \left[\begin{array}{cc|c} & & 0_{2\times 1} \\ & I_{2\times 2} & 1 \\ -\frac{1}{M} J_{12} & & 0 \\ & & 0 \\ & & 0 \end{array}\right] \left[\begin{array}{c} \lambda_x \\ \lambda_z \\ \hline \lambda_\psi \end{array}\right]. \tag{14}$$

2.6. Equations of motion at Stance II, Flight II and Touchdown II

Equations for Stance II, Flight II and Touchdown II can be obtained easily by swapping the angle coordinates $(\psi_1, \psi_2, \psi_3, \psi_4) \longleftrightarrow (\psi_4, \psi_3, \psi_2, \psi_1)$ in the equations.

3. BACK HANDSPRING CONTROLLER

3.1. Reference model

The back handspring is a rapid and complex motion task comprising multiple phases. In the control problem, it is unrealistic to depend on some pre-planned reference trajectories because, in general, such a trajectory-tracking scheme cannot adapt to environmental changes, which are difficult to predict. Instead, we attempt to achieve complex motion tasks by describing a simple reference model (equation of motion) about global physical quantities, such as the CM position or angular momentum around the CM.

Our method describes a reference model of hopping, somersaults and handsprings using common 'spring dynamics' in the 'stance phase'. Spring-like behavior of running is well known [12]; some examples exist in which spring-like behavior is imposed for controlling running robots [13]. Spring-like dynamics are useful when humans need to preserve mechanical energy during dynamic motion because they have tendons in their joints. In a hopping or running motion, humans can utilize their joint tendons to store the energy, which engenders reduction of power consumption. With appropriate parameters, tendon-driven running or hopping will generate spring-like behavior [1, 12]. In other words, spring-like dynamics are well suited to a tendon-driven mechanism. Discussions about how to introduce tendons into the articulated model are beyond the scope of this paper (but see Ref. [14], for example).

However, there are reasons why this paper gives a refrence model only to the stance phase. First, some floor exercises, such as the back handspring, do not have

sufficient flight time. When the flight period is short, the robot behavior in the flight phase is almost determined by the terminal state of the stance phase. Second, the model matching condition for spring dynamics is met only at the stance phase. There is no ground reaction force available in the flight phase and the robot cannot control the CM.

If sufficient flight time is available, it becomes important to control the terminal state of the robot within a given flight time. If the lift-off configuration lies in some accessible region for a given flight time, the posture can be steered to some desired region until the next touchdown. This problem leads to non-holonomic attitude control. A long-jump or somersault involves this kind of attitude control in the aerial phase. Basically, the posture can be controlled by actively controlling the moment of inertia around the CM [2]. Derivation of the controller, as well as the identification of its accessible region, is rather easy for an articulated two-link model [15]. However, for the three or more linked model, it becomes more difficult to analyze the model and derive controllers [16, 17]. This paper does not discuss the non-holonomic controller; it will be introduced in future work, where other interesting gymnastic motions with longer flight time, such as somersaults, will be realized by the robot.

Below, we define the reference model for the back handspring.

3.1.1. Stance I. At Stance I with the heel supporting, the reference models are designed as:

$$M\ddot{\overline{x}}_{\mathrm{g}} = a_1, \tag{15}$$

$$M\ddot{\overline{z}}_{\mathrm{g}} = -K_z(\overline{z}_{\mathrm{g}} - z_{\mathrm{e1}}), \tag{16}$$

$$\dot{\overline{P}}_{\mathrm{g}} = -K_{\mathrm{p}}(\overline{P}_{\mathrm{g}} - P_{\mathrm{gd}}), \tag{17}$$

where the 'barred' variables imply those of reference model dynamics to be followed by the controller in Section 3.2. The first two parts define spring-like dynamics of the CM, where a is the acceleration and z_{e1} is the virtual equilibrium. The last equation is the exponential convergence of P_{g}, the angular momentum around CM, to a desired value P_{gd}.

When the heel leaves the ground, the robot stands on its toe. There is no applied torque available around the contact point. In particular, we cannot control P_{g} arbitrarily in this phase because of the relationship:

$$\frac{\mathrm{d}}{\mathrm{d}t}P_{\mathrm{g}} = Mgr\sin\theta, \tag{18}$$

where r is the distance between the CM and toe, and θ is the angle. Therefore, (17) is abandoned and the reference model in this phase becomes

$$M\ddot{\overline{x}}_{\mathrm{g}} = a_1, \tag{19}$$

$$M\ddot{\overline{z}}_{\mathrm{g}} = -K_z(\overline{z}_{\mathrm{g}} - z_{\mathrm{e1}}). \tag{20}$$

3.1.2. Stance II. As in the case of toe contact in Stance I, reference models are set only to CM:

$$M\ddot{\overline{x}}_{\mathrm{g}} = a_2, \tag{21}$$

$$M\ddot{\overline{z}}_{\mathrm{g}} = -K_z(\overline{z}_{\mathrm{g}} - z_{\mathrm{e}2}). \tag{22}$$

3.1.3. Flight I and Flight II. There are no reference models designed for the flight phase in the back handspring. Instead, joint angles are controlled locally to a specified target configuration ($\psi_{\mathrm{d}} = \psi_{2\mathrm{d}}, \psi_{3\mathrm{d}}, \psi_{4\mathrm{d}}$) until the top of the link 4 (head) touches down.

3.2. Model matching control

This section derives model matching control input τ to realize the above reference model. Using this controller, the robot becomes dynamically equivalent to the reference model.

Substituting (15) and (16) into (8) yields:

$$\underbrace{E_{\mathrm{g}}J_{\mathrm{g}}^{-1}}_{A}(u - H_{\mathrm{g}} - G_{\mathrm{g}}) = \underbrace{-\gamma - \left(E_{\mathrm{g}}J_{\mathrm{g}}E_{\mathrm{g}}^{\mathrm{T}}\right)\begin{bmatrix} a_1 \\ -K_z(\overline{z}_{\mathrm{g}} - z_{\mathrm{e}1}) + Mg \\ \lambda_\psi \end{bmatrix}}_{B}, \tag{23}$$

or:

$$\begin{bmatrix} A_1 & A_2 \end{bmatrix}\left(\begin{bmatrix} 0_{3\times 1} \\ \tau \end{bmatrix} - H_{\mathrm{g}} - G_{\mathrm{g}}\right) = B, \tag{24}$$

where $A_1 \in R^{3\times 3}$, $A_2 \in R^{3\times 3}$ and $B \in R^3$. Rearranging this equation gives:

$$A_2\tau = B + A(H_{\mathrm{g}} + G_{\mathrm{g}}). \tag{25}$$

Therefore, if we specify λ_ψ in (23), the control input τ can be uniquely determined.

It is shown below that λ_ψ is related to the angular momentum. With the kinetic energy $K = \frac{1}{2}\dot{q}_{\mathrm{g}}^{\mathrm{T}}J_{\mathrm{g}}\dot{q}_{\mathrm{g}}$, the angular momentum P_{g} can be obtained by:

$$P_{\mathrm{g}} = \frac{\partial K}{\partial \dot{\psi}_1}, \tag{26}$$

because ψ_1 is the cyclic variable [11]. This equation results in:

$$P_{\mathrm{g}} = J_{\mathrm{g}33}\dot{\psi}_1 + J_{\mathrm{g}34}\dot{\psi}_2 + J_{\mathrm{g}35}\dot{\psi}_3 + J_{\mathrm{g}36}\dot{\psi}_4, \tag{27}$$

where $J_{\mathrm{g}3i}$ ($i = 3, 4, 5, 6$) shows the elements of the third row of J_{g} (see Appendix). Its time derivative is calculated as:

$$\dot{P}_{\mathrm{g}} = J_{\mathrm{g}33}\ddot{\psi}_1 + J_{\mathrm{g}34}\ddot{\psi}_2 + J_{\mathrm{g}35}\ddot{\psi}_3 + J_{\mathrm{g}36}\ddot{\psi}_4 - H_{\psi 1}(q_{\mathrm{g}}, \dot{q}_{\mathrm{g}}), \tag{28}$$

where $H_{\psi 1}(q_g, \dot{q}_g)$ is the first element of H_ψ in (9). Substituting the reference model (17) into this equation yields:

$$[\, J_{g33}\ J_{g34}\ J_{g35}\ J_{g36}\,]\ddot{\psi} = -K_p(\overline{P}_g - P_{gd}) + H_{\psi 1}. \tag{29}$$

On the other hand, the lower part of (9) gives:

$$[\, J_{g33}\ J_{g34}\ J_{g35}\ J_{g36}\,]\ddot{\psi} = H_{\psi 1} - \frac{1}{M} J_{12} \begin{bmatrix} \lambda_x \\ \lambda_z \end{bmatrix} + \lambda_\psi. \tag{30}$$

Thus, combining (29) with (30), then substituting (15) and (16), we can obtain the relationship between λ_ψ and the reference model about P_g:

$$\lambda_\psi = \frac{1}{M} J_{12} \begin{bmatrix} a_1 \\ -K_z(\overline{z}_g - z_{e1}) + Mg \end{bmatrix} - K_p(\overline{P}_g - P_{gd}). \tag{31}$$

However, in the case of toe contact in Stance I, or Stance II, λ_ψ dissappears in (23), and the dimensions of A and B shrink; $A_1 \in R^{2\times 3}$, $A_2 \in R^{2\times 3}$ and $B \in R^2$. In this case, although the model matching condition still holds, control inputs cannot be chosen 'uniquely' because A_2 is non-invertible. Therefore, the pseudo-inverse $A_2^{\#} = A_2^{\mathrm{T}}(A_2 A_2^{\mathrm{T}})^{-1}$ is introduced.

4. SIMULATION AND EXPERIMENT

The parameters to be determined are:

- Initial configuration $\psi(0)$
- a_1, K_z, z_{e1}, P_{gd}, a_2, z_{e2} (Stance I and Stance II)
- Desired touchdown posture ψ_d (Flight I and Flight II).

Moreover, we should consider the joint torque limit of ± 1.5 Nm.

These parameters are roughly tuned at this first stage. A reasonable way to find the parameters is an ongoing task (see Section 5). However, for reference, we describe how we get feasible parameters for back handsprings step by step. First, $\psi(0)$ is determined from $x_g(0)$ and $z_g(0)$, where $x_g(0)$ is set to the same horizontal position of the ankle joint. Then, $z_g(0)$, a_1, K_z, z_{e1} and P_{gd} in Stance I are tuned so that the robot touches down on the ground as soon as possible, thereby shortening the flight time. For that reason, we can choose ψ_d as the terminal position of Stance I. If angular momentum P_g has a sufficiently high level, it is easy for the robot to rotate around its pivot (head) in Stance II. We first try to set P_{gd} to some constant value to be reached, but the results are unsatisfactory; the robot rotates much more quickly than the translational motion of (x_g, z_g). Therefore, we modify it by:

$$P_{gd} = -c\left(x_g - x_g(0)\right), \tag{32}$$

where c is a constant. This comes from our observation that a gymnast increases his rotational speed when the horizontal position of the CM proceeds sufficiently.

The parameters in Stance II are difficult to choose. The difficulty arises from the underactuated structure of Stance II: P_g can not be controlled arbitrarily in this phase, as described in A.1). This fact implies that we cannot expect enough P_g at the second lift-off (if the robot has arms with shoulder joints, the controllability will be greatly increased. This will be done in our next stage). Therefore, we set z_{e2} and K_{z2} larger than those of Stance I to make the robot take off higher. The higher the robot jumps, the more flight time is available for controlling the final configuration, even if P_g is not sufficient. The final parameter ψ_d in Flight II is tuned so that the robot can stop and stand still.

Table 2 shows one parameter that is set in that manner. Using these parameters, a successful back handspring motion is performed in both the simulation and experiment. Figures 5 and 6 show the time evolution of each joint angle and joint torque, together with the On/Off state of the ground contact (On = 1, Off = 0) at the simulation and experiment. In this experiment, the On/Off state is determined by microswitches installed under the mat; each joint torque is obtained by motor current via an AD converter. The robot does not contain a high-speed gyro (more than 1000°/s). Therefore, the commanded torque is determined by simulation, except for the PD-feedback in the two flight phases and the final phase (stopping the motion).

Figure 7 depicts an animation created by simulation; Fig. 8 shows snap shots of the corresponding experiment, where the sequence of Touchdown I, Lift-off I and Touchdown II is captured clearly.

Although the back handspring finishes within a very short period of time (around 0.6 s), the behavior of the robot, as well as phase transitions, are captured clearly in the graphs and videos. From 0.0 to 0.2 s, the robot contacts the ground with its feet. From 0.2 to 0.3 s, the robot contacts the ground with its toes. Figure 6 shows that the joint torques are saturated in this phase, regardless of the 'optimal' torque distribution by pseudo-inverse. This demonstrates the difficulty of controlling the CM without a foot: the robot requires maximum torque to follow the reference model.

Until the first touchdown (0.3 s), there are no marked differences between the simulation and experiment: the model identification is almost perfect. However, the differences become larger after the touchdown. The most remarkable difference is

Table 2.
Control parameters

Parameter	Unit	Value
$\psi_2(0)$, $\psi_3(0)$, $\psi_4(0)$	deg	120, −94, 90
a_1, z_{e1}, K_z, c at Stance I	—	4.5, 0.19, 20, 4.2
a_2, z_{e2}, K_z at Stance II	—	3.8, 0.56, 40
ψ_{1d}, ψ_{2d}, ψ_{3d} at Flight I	deg	0, −70, −100
ψ_{1d}, ψ_{2d}, ψ_{3d} at Flight II	deg	133, −129, 120

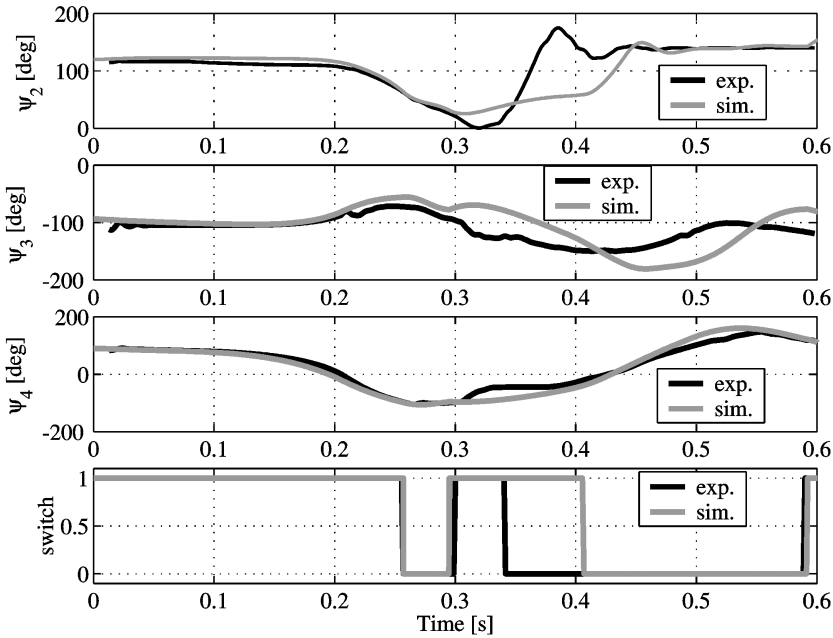

Figure 5. Joint angles in the simulation and experiment.

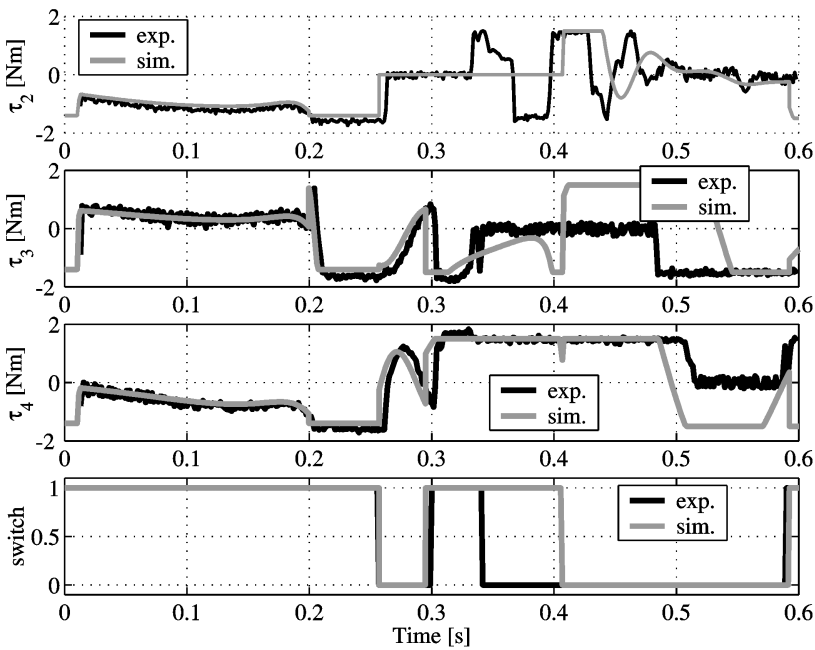

Figure 6. Joint torques in the simulation and experiment.

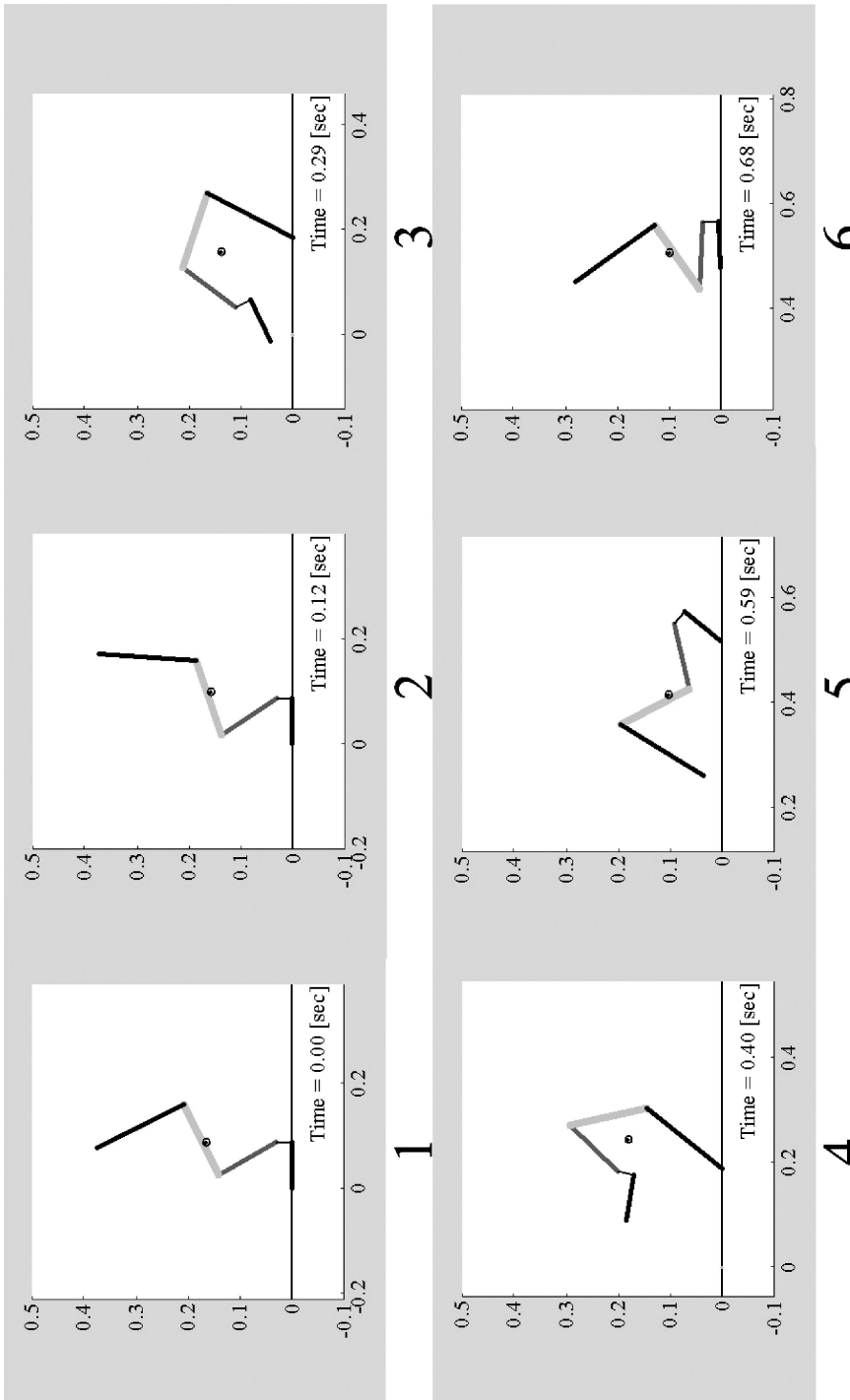

Figure 7. Stick animation of the back handspring simulation corresponds to the data in Figs 5 and 6.

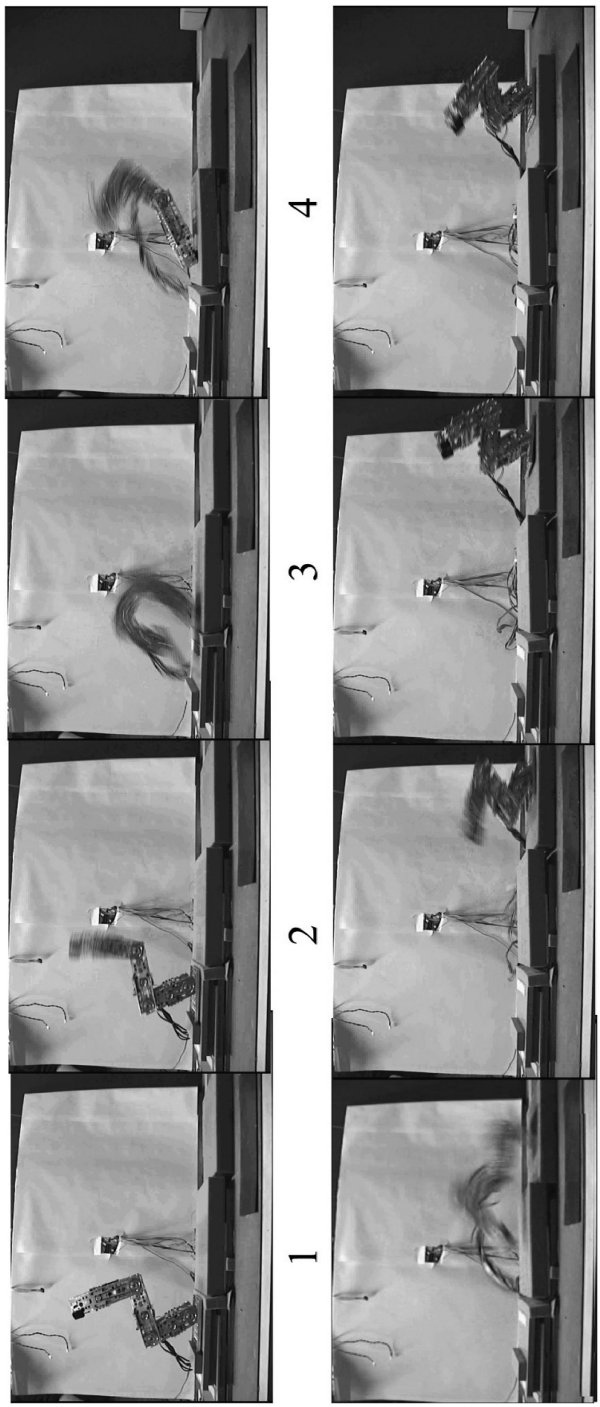

Figure 8. Snap shots of the back handspring experiment corresponding to data in Figs 5 and 6; the index numbers correspond to those of Fig. 7, but the time stamps do not coincide after no. 4.

the period of Stance II. The stance period of the simulation is about 0.1 s, whereas that of the experiment is about 0.05 s. This fact implies that the difference mainly arises from the modeling error of the touchdown phase; apparently, the mat covering the floor does not emulate the inelastic impulse assumption well. The stance period affects the spring dynamics, especially for vertical motion. If the period is too short, the vertical speed of the CM cannot be restored. For this reason, the ground level at the final landing is slightly lower than the starting level. However, the modeling error can be overcome by installing hands, by which spring dynamics should be followed at Stance II, as in Stance I. Although the experiment can be successful only by such on-the-spot tuning, the repeatability of the experiment is very high except for its termination (we do not use active balancing control).

5. CONCLUSION

This paper proposed a control framework and a robotic test bed to study skill control in gymnastic motions by presenting a specific example — a back handspring motion. For this purpose, a planar and serially connected four-link robot was developed. Its joints are actuated by electric servomotors. Then a control framework for fast and complex gymnastic motion was proposed. It comprised a task-specific reference model and model matching control; it differs from the classical control method that requires pre-planned reference trajectories. The use of global physical quantities such as the CM or angular momentum allowed even a simple reference model to generate complex gymnastic motions of a multi-body system. The effectiveness of the controller was confirmed *via* simulations and experiments using a back handspring motion. This is the first time that a back handspring has been performed by a real multi-link robot.

However, this is our first stage. Two main tasks remain for future work:

(i) Touchdown control to give appropriate initial angular momentum for the next stance phase.

(ii) Systematic design of the control parameter or re-design of the reference model.

The first task will lead to stability of the floor exercise. As stated in Section 2, reference models in the air are not provided in this paper because they are not necessary for the back handspring motion. Thereby, we have succeeded in performing a back handspring without active posture control at the flight phase. The only exception will be control of the touchdown position of the foot (or hand). The touchdown position governs the dominant rotational behavior at the stance phase because the torque around the toe is not available; alternatively, the torque of the ankle joint (or wrist joint) is limited by the zero-moment point. Controlling the touchdown position leads to 'gait stability' of the consecutive handspring motion or it helps to terminate the gymnastic motion. Instead of controlling all states using a non-holonomic attitude controller, it will be rather realistic to give priority to the touchdown position. For those reasons, derivation of the controller is our next step.

The second task poses the most important problem because it includes the key to skill control. A general solution to determine control parameters such as virtual spring constant or desired angular momentum according to specific gymnastic motions is needed. In this context, re-design of the reference model should also be considered as an alternative.

After solving these two problems, a non-holonomic attitude controller at the flight phase will be combined effectively with the stance controller and used for the gymnastic motions with a longer flight time.

Acknowledgements

This study was partially supported by the Ministry of Education, Science, Sports and Culture, Grant-in-Aid for Young Scientists (B), 15760144, 2003. The authors thank Masatoshi Suzuki for his help in fabricating the hardware.

REFERENCES

1. M. Raibert, *Legged Robots That Balance.* MIT Press, Cambridge, MA (1985).
2. J. Hodgins and M. Raibert, Biped gymnastics, *Int. J. Robotics Res.* **9**.
3. K. Arikawa and T. Mita, Design of multi-dof jumping robot, in: *Proc. IEEE Int. Conf. on Robotics and Automation*, Washington, DC, pp. 3992–3997 (2002).
4. M. Spong, The swing up control problem for the acrobot, *IEEE Control Syst. Mag.* **15**, 49–55 (1995).
5. M. Yamakita, T. Yonemura, Y. Michitsuji and Z. Luo, Stabilization of acrobot in upright position on a horizontal bar, in: *Proc. IEEE Int. Conf. on Robotics and Automation*, Washington, DC, pp. 3093–3098 (2002).
6. J. Nakanishi, T. Fukuda and D. Koditschek, A brachiating robot controller, *IEEE Trans. Robotics Automat.* **16**, 109–123 (2000).
7. M. Yamakita, M. Kishikawa and T. Sadahiro, Motion control for robust landing of acrobat robot (smb), in: *Proc. IEEE/RSJ Int. Conf. on Intelligent Robots and Systems*, Las Vegas, NV, pp. 1141–1146 (2003).
8. M. Berkemeier and R. Fearing, Tracking fast inverted trajectories of the underactuated acrobot, *IEEE Trans. Robotics Automat.* **15**, 740–750 (1999).
9. M. Miyazaki, M. Sampei and M. Koga, Control of the motion of an acrobot approaching a horizontal bar, *Advanced Robotics* **15**, 467–480 (2001).
10. S. Hyon, N. Yokoyama and T. Emura, Back handspring control of a multi-link gymnastic robot, in: *Proc. 3rd IFAC Symp. on Mechatronic Systems*, Sydney, pp. 73–38 (2004).
11. D. T. Greenwood, *Classical Dynamics*. Prentice-Hall, Englwood Cliffs, NJ (1977).
12. C. T. Farley, J. Glasheen and T. A. McMahon, Running springs: speed and animal size, *J. Exp. Biol.* **185**, 71–86 (1993).
13. T. Ikeda, T. Tamura and T. Mita, Development and running control of a 3d leg robot, in: *Proc. of AMAM*, Kyoto (2000).
14. S. Hyon and T. Mita, Development of a biologically-inspired hopping robot — kenken, in: *Proc. IEEE Int. Conf. on Robotics and Automation*, Washington, DC, pp. 3984–3991 (2002).
15. T. Mita, S. Hyon and T. Nam, Analytical time optimal control solution for a two link planar acrobot with initial angular momentum, *IEEE Trans. Robotics Automat.* **17**, 361–366 (2001).

16. J. Godhavn, A. Balluchi, L. Crawford and S. Sastry, Steering of a class of nonholonomic systems with drift terms, *Automatica* **35**, 837–847 (1999).
17. M. Sampei, H. Kiyota and M. Ishikawa, Control strategies for mechanical systems with various constraints, in: *Proc. IEEE Conf. on Systems, Man and Cybernetics*, Tokyo, pp. 158–167 (1999).

APPENDIX: DERIVATION OF EQUATION OF MOTION WITHOUT CONSTRAINT

The appendix provides details of equations of motion without constraints. These are the flight phase dynamics. Presuming the kinetic energy of the robot as $K = (1/2)\dot{q}^{\mathrm{T}} J(q)\dot{q}$, the coordinate transformation from $q = [x_0, z_0, \psi]^{\mathrm{T}}$ to $q_{\mathrm{g}} = [x_{\mathrm{g}}, z_{\mathrm{g}}, \psi]^{\mathrm{T}}$ is performed as:

$$K = \frac{1}{2}\dot{q}^{\mathrm{T}} J(q)\dot{q} = \frac{1}{2}\dot{q}_{\mathrm{g}} R(\psi)^{\mathrm{T}} J(q) R(\psi)\dot{q}_{\mathrm{g}} = \frac{1}{2}\dot{q}_{\mathrm{g}} J_{\mathrm{g}}(\psi)\dot{q}_{\mathrm{g}}, \tag{A.1}$$

where $R(\psi) := \frac{\partial q}{\partial q_{\mathrm{g}}}$ is the transformation matrix. Since the CM position can be calculated as:

$$\begin{bmatrix} x_{\mathrm{g}} \\ z_{\mathrm{g}} \end{bmatrix} = \begin{bmatrix} x_0 \\ z_0 \end{bmatrix} - \frac{1}{M}\begin{bmatrix} b_1 C_1 + b_2 C_{12} + b_3 C_{123} + b_4 C_{1234} \\ b_1 S_1 + b_2 S_{12} + b_3 S_{123} + b_4 S_{1234} \end{bmatrix}, \tag{A.2}$$

where:

$$\begin{aligned} M &= m_1 + m_2 + m_3 + m_4 \\ b_1 &= -m_1 l_{\mathrm{c}1} - (m_2 + m_3 + m_4) l_1 \\ b_2 &= -m_2 l_{\mathrm{c}2} - (m_3 + m_4) l_2 \\ b_3 &= -m_3 l_{\mathrm{c}3} - m_4 l_3 \\ b_4 &= -m_4 l_{\mathrm{c}4} \\ S_{12\ldots} &= \sin(\psi_1 + \psi_2 + \cdots) \\ C_{12\ldots} &= \cos(\psi_1 + \psi_2 + \cdots) \end{aligned}$$

the transformation matrix $R(\psi)$ can be represented as:

$$R(\psi) = \left[\begin{array}{cc|c} 1 & 0 & \\ 0 & 1 & -\frac{1}{M} J_{12} \end{array}\right] \in R^{2\times 6}, \tag{A.3}$$

where:

$$J_{12} = \begin{bmatrix} -b_1 S_1 & -b_2 S_{12} & -b_3 S_{123} & -b_4 S_{1234} \\ b_1 C_1 & b_2 C_{12} & b_3 C_{123} & b_4 C_{1234} \end{bmatrix} \in R^{2\times 4}, \tag{A.4}$$

is the submatrix of $J(q)$, the inertia matrix of the toe coordinate system.

Inertial matrix $J_g(\psi)$ in (A.1) is calculated as the following.

$$J_g(\psi) = \left[\begin{array}{cc|cccc} M & 0 & 0 & 0 & 0 & 0 \\ 0 & M & 0 & 0 & 0 & 0 \\ \hline 0 & 0 & J_{g33} & J_{g34} & J_{g35} & J_{g36} \\ 0 & 0 & J_{g34} & J_{g44} & J_{g45} & J_{g46} \\ 0 & 0 & J_{g35} & J_{g45} & J_{g55} & J_{g56} \\ 0 & 0 & J_{g36} & J_{g46} & J_{g56} & J_{g66} \end{array}\right] \in R^{6\times 6}, \tag{A.5}$$

$$\begin{aligned}
J_{g33} &= 2(k_5C_2 + k_6C_3 + k_7C_4 + k_8C_{23} + k_9C_{34} + k_{10}C_{234} \\
&\quad + k_{11}S_2 + k_{12}S_{23} + k_{13}S_{234}) + k_1 + k_2 + k_3 + k_4 + k_{14}, \\
J_{g34} &= k_5C_2 + 2k_6C_3 + 2k_7C_4 + k_8C_{23} + 2k_9C_{34} + k_{10}C_{234} \\
&\quad + k_{11}S_2 + k_{12}S_{23} + k_{13}S_{234} + k_4 + k_2 + k_3, \\
J_{g35} &= k_6C_3 + 2k_7C_4 + k_8C_{23} + k_9C_{34} + k_{10}C_{234} \\
&\quad + k_{12}S_{23} + k_{13}S_{234} + k_4 + k_3, \\
J_{g36} &= k_7C_4 + k_9C_{34} + k_{10}C_{234} + k_{13}S_{234} + k_4, \\
J_{g44} &= 2k_6C_3 + 2k_7C_4 + 2k_9C_{34} + k_2 + k_3 + k_4, \\
J_{g45} &= k_6C_3 + 2k_7C_4 + k_9C_{34} + k_3 + k_4, \\
J_{g46} &= k_7C_4 + k_9C_{34} + k_4, \\
J_{g55} &= 2k_7C_4 + k_3 + k_4, \\
J_{g56} &= k_7C_4 + k_4, \\
J_{g66} &= k_4, \\
k_1 &= (Ma_{11} - b_1^2)/M, \\
k_2 &= (Ma_{22} - b_2^2)/M, \\
k_3 &= (Ma_{33} - b_3^2)/M, \\
k_4 &= (Ma_{44} - b_4^2)/M, \\
k_5 &= (Ma_{12} - b_5b_2)/M, \\
k_6 &= (Ma_{14} - b_2b_3)/M, \\
k_7 &= (Ma_{23} - b_4b_3)/M, \\
k_8 &= (Ma_{13} - b_5b_3)/M, \\
k_9 &= (Ma_{45} - b_2b_4)/M, \\
k_{10} &= (Ma_{24} - b_5b_4)/M, \\
k_{11} &= (Ma_{25} + b_1b_2)/M, \\
k_{12} &= (Ma_{34} + b_1b_3)/M, \\
k_{13} &= (Ma_{35} + b_1b_4)/M, \\
k_{14} &= (Ma_h - b_5^2)/M, \\
b_5 &= -(m_2 + m_3 + m_4)h,
\end{aligned}$$

$$
\begin{aligned}
a_{12} &= (m_2 l_{c2} + m_3 l_2 + m_4 l_2)h, \\
a_{13} &= (m_3 l_{c3} + m_4 l_3)h, \\
a_{14} &= (m_3 l_{c3} + m_4 l_3)l_2, \\
a_{23} &= m_4 l_{c4} l_3, \\
a_{24} &= m_4 l_{c4} h, \\
a_{25} &= -(m_2 l_{c2} + m_3 l_2 + m_4 l_2)l_1, \\
a_{34} &= -(m_3 l_{c3} + m_4 l_3)l_1, \\
a_{35} &= -m_4 l_{c4} l_1, \\
a_{11} &= J_1 + m_1 l_{c1}^2 + (m_2 + m_3 + m_4)l_1^2, \\
a_{22} &= J_2 + m_2 l_{c2}^2 + (m_3 + m_4)l_2^2, \\
a_{33} &= J_3 + m_3 l_{c3}^2 + m_4 l_3^2, \\
a_{44} &= J_4 + m_4 l_{c4}^2, \\
a_{45} &= m_4 l_{c4} l_2, \\
a_h &= (m_4 + m_3 + m_2)h^2.
\end{aligned}
$$

Then, with the new CM-coordinate system, Lagrange's equation of motion, in which potential energy U depends on the generalized coordinate only, is described as:

$$
\frac{\mathrm{d}}{\mathrm{d}t}\left(\frac{\partial K}{\partial \dot{q}_\mathrm{g}}\right) - \underbrace{\frac{\partial K}{\partial q_\mathrm{g}}}_{h_{\mathrm{g}2}(q_\mathrm{g}, \dot{q}_\mathrm{g})} + \underbrace{\frac{\partial U}{\partial q_\mathrm{g}}}_{G_\mathrm{g}(q_\mathrm{g})} = u, \tag{A.6}
$$

where the first term is calculated from (A.1):

$$
\frac{\mathrm{d}}{\mathrm{d}t}\left(\frac{\partial K}{\partial \dot{q}_\mathrm{g}}\right) = J_\mathrm{g}(q_\mathrm{g})\ddot{q}_\mathrm{g} + \underbrace{\frac{\mathrm{d}}{\mathrm{d}t} J_\mathrm{g}(q_\mathrm{g})\dot{q}_\mathrm{g}}_{h_{\mathrm{g}1}(q_\mathrm{g}, \dot{q}_\mathrm{g})}. \tag{A.7}
$$

Therefore, we obtain:

$$
J_\mathrm{g}(q_\mathrm{g})\ddot{q}_\mathrm{g} + H_\mathrm{g}(q_\mathrm{g}, \dot{q}_\mathrm{g}) + G_\mathrm{g}(q_\mathrm{g}) = u, \tag{A.8}
$$

where $H_\mathrm{g}(q_\mathrm{g}, \dot{q}_\mathrm{g}) = (h_{\mathrm{g}1}(q_\mathrm{g}, \dot{q}_\mathrm{g}) - h_{\mathrm{g}2}(q_\mathrm{g}, \dot{q}_\mathrm{g}))$ is the non-linear term, which includes the centrifugal force, and Coriolis force and $G_\mathrm{g}(q_\mathrm{g})$ is the gravity term. They have the following decomposed structure:

$$
H_\mathrm{g}(q_\mathrm{g}, \dot{q}_\mathrm{g}) = \begin{bmatrix} 0 \\ 0 \\ H(\psi) \end{bmatrix} \in R^6, \tag{A.9}
$$

$$G_{\mathrm{g}}(q_{\mathrm{g}}) = \begin{bmatrix} 0 \\ Mg \\ 0_{(4\times 1)} \end{bmatrix} \in R^6. \tag{A.10}$$

We do not show the each element of $H_{\mathrm{g}}(q_{\mathrm{g}}, \dot{q}_{\mathrm{g}})$. It can be easily obtained by (A.5), (A.7) and (A.8), using any symbolic manipulation tool such as Maple V or Mathematica. The joint-wise friction term $W\dot{q}_{\mathrm{g}}$ is not shown here, but is identified and compensated for in the experiment.

ABOUT THE AUTHORS

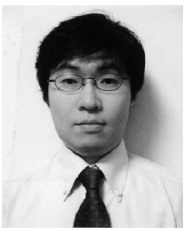

Sang-Ho Hyon received the ME degree from Waseda Univerisity in 1998 and the PhD degree from Tokyo Institute of Technology in 2002. He is currently an Assistant Professor in the Department of Bioengineering and Robotics, Tohoku University. His research interests are dynamic legged locomotion, non-linear oscillation, etc. He is a member of the RSJ, SICE and IEEE.

Naoto Yokoyama received the ME degree from the Department of Bioengineering and Robotics, Tohoku University in 2004. He is currently with the Department of EMD, Makino Corp. His research interest is robotic systems. He is a member of the RSJ.

Takashi Emura received the PhD degree from Tohoku University in 1969. He is currently a Professor in the Department of Bioengineering and Robotics, Tohoku University. During 1972–1973, he succeeded in walking a biped dynamically and found that the semicircular canal should be defined as an angular velocity sensor. His research interests include legged robots, automatic navigation vehicles, high-precision servomechanisms for numerically controlled machines, etc. He is a member of the RSJ, JSME, SICE, JSPE and IEEE.